EPMA Measurements of Diffusion Profiles at the Submicrometre Scale

Olivier Arnould, François Hild

Title. EPMA Measurements of Diffusion Profiles at the Submicrometre Scale.

Authors. Olivier ARNOULD*, François HILD

LMT-Cachan, ENS de Cachan / CNRS-UMR 8535 / Université Paris VI

61 avenue du Président Wilson, F-94235 Cachan Cedex, France

Abstract. Concentration profiles due to (inter)diffusion in materials may require high spatial resolution. These profiles may be measured by electron probe microanalysis, which allows one to determine the elemental composition with a good accuracy provided measurement 'artefacts' can be accounted for. Standard phenomena are usually corrected by commercial softwares that assume a homogeneous elemental composition in the analysed area. However, in the case of a diffusion process on a small scale, the composition is no longer homogeneous and the effect of the hemispherical volume of the X-ray emission on the spatial resolution of the concentration profiles, and consequently on the diffusion coefficients, has to be considered. Moreover, (secondary) fluorescence across interfaces or interphases has to be evaluated. A radial X-ray distribution associated with the characteristic depth distribution, $\phi(\rho z)$, allows for the definition of a 2D X-ray emission function that enables the computation of the entire process for a given concentration profile.

Key words. EPMA, concentration profiles, average effect, (secondary) fluorescence, interface.

Introduction: measurement of concentration profiles obtained by diffusion.

The evaluation of diffusion coefficients may require high spatial resolution. One of the easiest and most reliable techniques is the Electron Probe MicroAnalysis (EPMA). It is based on measuring the relative intensities of the X-ray wavelengths (WDS), or energies (EDS), emitted by a sample impacted by an electron beam. It allows for the identification and quantification of elemental compositions and chemical compounds if a variety of interactions between electrons, X-rays and atoms are accounted for. The main factors are now well-understood and readily corrected by ZAF or $\phi(\rho z)$ methods for a uniform concentration in the area probed by the electrons and X-ray diffusion in the sample. For non-homogeneous chemical compounds, *i.e.*, when a phase boundary is present within the volume affected by the electrons or the emitted X-rays, specific phenomena occur. They are summarised in Fig. 1 in which a 1D varying concentration between two pure elements, say A and B with $\mathrm{Z_B} > \mathrm{Z_A}$, along Y only is considered. The concentration gradient is described by the mass fraction in A, $\mathrm{C_A}(Y)$, and is depicted by the grey level in Fig. 1; the darker, the richer in A-atoms. The origin of this profile, O,

corresponds to the position of an ideal interface before diffusion has occurred (becoming an interphase between A and B elements when diffusion occurred). The B-rich phase is located for $Y \leq 0$ so that $\mathrm{C_A}(Y)$ increases with Y. The primary electron beam (accelerating voltage $\mathrm{E_0}$) is focused at point I on the surface sample, at a distance $Y = \mathrm{d}$ from the initial interface.

The first effect is due to the electron diffusion in the specimen that produces a characteristic emission function whose shape is close to a hemisphere of average radius R_X for medium to high Z materials (Fig. 2). The measurement corresponds to an average over this volume leading to what will be referred to as average effect. When dealing with diffusion couples, it has to be evaluated when the diffusion length (*i.e.*, the distance over which diffusion has occurred) is of the order of a characteristic length of the hemispherical emission volume, *i.e.*, when $\sqrt{2Dt} \approx R_\mathrm{X}$, where D is the average diffusion coefficient and t the diffusion time. Furthermore, each part $\mathrm{d}y\,\mathrm{d}z$ of the emission volume in S emits characteristic and continuous X-rays in all directions that travel through the specimen to reach a point M. Along its way, the radiation is absorbed in an exponential fashion with a varying attenuation coefficient and can excite A-atoms at M leading to (secondary) fluorescence that is measured and modifies the analysed spectra. The volume concerned by this effect is much larger than that of the primary radiation and can be predominant at a longer range. Classical correction methods take this effect into account for a homogeneous volume but not when different phases or multilayered materials are present. Finally, the primary and secondary X-rays travel towards the spectrometer in a varying composition from M to the surface at N for the latter, and from S to N' for the former. This phenomenon introduces a specific absorption correction that is controlled by the detection geometry (take-off angle θ and orientation of the interface with respect to the spectrometer δ). The emissions of primary radiation of A and B elements from the elementary point source S that are detected by the spectrometer for $\varphi = \delta + \pi/2$ and $\psi = \theta + \pi/2$ are shown in Fig. 1.

Average effect

A 2D characteristic distribution function of primary X-rays

Previous studies on the resolution of EPMA techniques [1, 2, 3], Monte Carlo simulations [4][1] of the X-ray emission distribution together with the change in intensities when crossing an ideal interface, lead us to assume that the distribution function, in the local co-ordinates (I, x, y, z), is close to (Fig. 2)

$$F(r, z) = g_\sigma(r)\, \phi(\rho z), \tag{1}$$

where $r^2 = x^2 + y^2$ and $g_\sigma(r)$ stands for a Gaussian distribution of standard deviation σ that describes the lateral spread of the electrons due to their random walk in the material [1, 5, 6]. This is an oversimplification of the real distribution, λ in Fig. 2, but it gives very satisfactory and simple results [3]. Since the evolution of the characteristic intensities across a 1D concentration gradient, along Y, between two pure materials is expected, the global computation, measured primary intensity and fluorescence (secondary excitation), is independent of x. The characteristic emission function only needs to be expressed in the two principal co-ordinates of the problem, namely the axis of concentration profile y and the sample depth z. Since the lateral distribution is described by a Gaussian function, integration over x leads to the same expressions as (1), in which r is replaced by y, for the 2D emission function in the (I, y, z) co-ordinates. In the last expression, it is assumed that the two distribution functions are *independent*. By integrating Eq. (1) over y leads to the well-known depth-distribution function $\phi(\rho z)$ since a Gaussian distribution has, by definition, a unit area. The model used to describe $\phi(\rho z)$ is the Gaussian proposed by Packwood and Brown [6, 7]. This model gives very acceptable results for most materials (*i.e.,* atomic number greater than ten) with the modified parameters [8, 9].

The lateral spread of the distribution function has been studied by several authors [1, 2, 5], and by Reed [3], but the first studies seem to overestimate R_{X} obtained by Monte Carlo simulations [10, 11, 12][2]. For most materials, the global shape of the X-ray emission volume is close to a hemisphere centred at z_{r} (Fig. 2). This corresponds to the point where the initially collimated electron beam leads to an entire scattering process. This can be used to relate the parameter of the lateral spread (lateral cut-off 3σ) to the maximum depth of the distribution. Another way is to consider that the electron spread is isotropic about the point z_{r}. The lateral spread is equal to the depth spread from z_{r} to ∞. This last approach seems to be consistent with the results obtain by Reed [3] (see also Ref. [13]) and is depicted in Fig. 2 as the function $\lambda(y)$. In some practical situations, the size of the beam diameter must be considered to evaluate the lateral spread in contrast to the depth behaviour which is far less affected. This is crucially important for WDS measurements since the probe diameter can be of the order of a typical electron path. A general equation exists to estimate this diameter [14] but the parameters involved in this formula are not well known in the present case. The parameter σ is adjusted by using the results of the next section. Finally, the intensity measured in a pure element (reference or standard), say B, can be expressed as

$$\mathrm{I}_{(\mathrm{B})} = \Delta \int_{z=0}^{\infty} \int_{y=-\infty}^{\infty} \phi(\rho z)\, g_\sigma(y) \exp\left(-\mu_{\mathrm{B}}^{\mathrm{B}}\, \rho_{\mathrm{B}} \frac{z}{\sin(\theta)}\right) \mathrm{d}\rho z\, \mathrm{d}y, \tag{2}$$

where $\mu_{\mathrm{B}}^{\mathrm{B}}$ is the mass attenuation coefficient in B for the considered B radiation, ρ_{B} the density of B, and Δ the coefficient including such parameters as beam current and spectrometer efficiency that disappear in any measurement relative to a standard sample [15].

Concentration profiles: deconvolution in a simplified case

Let us consider two materials that are initially separated by an ideal interface perpendicular to Y. These materials are about to diffuse and a concentration gradient takes place along Y. This part focuses on the average effect of the emission volume when its scale R_{X} is greater than or equal to the diffusion length. A similar situation was discussed by Lo *et al.* [16] and Ganguly *et al.* [17]. Fluorescence is not considered and some simplifications are performed to derive an *exact* formula to assess this 'artefact' [18]. The spectrometer position is such that $\delta = \pi/2$ in Fig. 1. Therefore, the measured emission has always travelled to the surface through a constant composition. The measured k-ratio of B for the beam impact position d in the concentration profile is

$$k_{\mathrm{B}}(\mathrm{d}) = \frac{\mathrm{I}_{\mathrm{B}}(\mathrm{d})}{\mathrm{I}_{(\mathrm{B})}} = \frac{\int_{z=0}^{\infty}\int_{y=-\infty}^{\infty} \phi^*(\rho z)\, g_\sigma^*(y)\, \mathrm{C}_{\mathrm{B}}(y+\mathrm{d}) \exp\left(-(\mu_{\mathrm{B}}^{\mathrm{AB}}\,\rho_{\mathrm{AB}})(y+\mathrm{d})\frac{z}{\sin(\theta)}\right) \mathrm{d}y\,\mathrm{d}\rho z}{\int_{z=0}^{\infty}\int_{y=-\infty}^{\infty} \phi(\rho z)\, g_\sigma(y) \exp\left(-\mu_{\mathrm{B}}^{\mathrm{B}}\,\rho_{\mathrm{B}}\frac{z}{\sin(\theta)}\right) \mathrm{d}y\,\mathrm{d}\rho z}, \quad (3)$$

where ϕ^* and g_σ^* stand for the distribution functions in the average concentration over the hemisphere in A and B elements at the position $Y = \mathrm{d}$ in the concentration gradient. The parameters of this distribution function have to be calculated by an *ad hoc* average formula such as the one proposed by Bastin *et al.* [19]. Since only close material couples (*i.e.,* with close atomic number and atomic weight) are considered (such as nickel/copper or zinc/nickel), the depth distribution is weakly modified by the presence of non-uniform material. Monte Carlo simulations of ϕ in various concentrations of A and B in a graded material show only negligible change in the overall shape for the materials of interest. Since the lateral spread of the electrons is similar to the depth one, the previous results apply for σ too. All these simplifications, and the above expression, will be used in the following part since they introduce a weak error in the global computation. When no diffusion occurs, the concentration gradient is equal to a concentration jump at $Y = 0$. It follows that Eq. (3) can be simplified and yields

$$k_{\mathrm{B}}(\mathrm{d}) = \int_{y=-\infty}^{-\mathrm{d}} g_\sigma(y)\mathrm{d}y = \frac{1}{2}\left[1 + \mathrm{erf}\left(-\frac{\mathrm{d}}{\sqrt{2}\sigma}\right)\right], \quad (4)$$

where *erf* denotes the error function. This equation is used to identify the standard deviation σ on a reference configuration of the materials, *i.e.,* two materials with an ideal interface without diffusion as shown in Fig. 3(a). The measurements are carried out with PGT EDS on HITACHI S510 SEM

for a Ni(A)/Cu(B) couple obtained by electroplating nickel onto a fine polished surface of copper followed by cutting and careful polishing of the complete assembly parallel to the interface. It must be remembered that the identification must be carried out on the part of the measurement that is the least affected by fluorescence, *i.e.*, on the intensity of the material B since it is only concerned by the continuum fluorescence arising from the background. When diffusion has occurred, the change of the absorption coefficient and density with the concentration is neglected, $(\mu_{\mathrm{B}}^{\mathrm{AB}}\,\rho_{\mathrm{AB}})(y+\mathrm{d}) \sim \mu_{\mathrm{B}}^{\mathrm{B}}\,\rho_{\mathrm{B}}$. This is an oversimplification that introduces a non-negligible error in the global computation but it yields a simple formula for the average effect. The part of this effect on the measurement of a diffusion coefficient can be rapidly assessed before any complex computation with a more realistic model. The different integrations over space, in Eq. (3), can be separated and the integrations over z cancelled. Under these assumptions, the measured mass fraction, $\mathrm{M_B}$, is equal to the k-ratio

$$\mathrm{M_B}(\mathrm{d}) = k_{\mathrm{B}}(\mathrm{d}) = \int_{y=-\infty}^{\infty} g_\sigma(y)\,\mathrm{C_B}(y+\mathrm{d})\,\mathrm{d}y = \int_{Y=-\infty}^{\infty} \mathrm{C_B}(Y)\,g_\sigma(\mathrm{d}-Y)\,\mathrm{d}Y = (\mathrm{C_B}\otimes g_\sigma)(\mathrm{d}), \quad (5)$$

where $\otimes$ denotes the convolution product. If the diffusion coefficient D is assumed to be independent of the concentration, the Fick's law combined with the equation of continuity (*i.e.*, conservation law) yields the diffusion equation that can be solved *exactly* by means of a Fourier transform. The concentration profile $\mathrm{C_B^t}$ at time t of the diffusion process can be then expressed as a convolution product

$$\mathrm{C_B^t}(\mathrm{d}) = (\mathrm{C_B^0}\otimes g_{\sqrt{2Dt}})(\mathrm{d}), \quad (6)$$

where $\mathrm{C_B^0}$ is the initial concentration profile, *e.g.*, when no diffusion occurred it is modelled by a step function. This expression clearly shows the similarity between the measurement (5) and a diffusion equation. Moreover, the raw measurement of the diffusion profile is given by

$$\mathrm{M_B}(\mathrm{d}) = (\mathrm{C_B^t}\otimes g_\sigma)(\mathrm{d}) = (\mathrm{C_B^0}\otimes g_\Sigma)(\mathrm{d}), \quad (7)$$

with $\Sigma = \sqrt{\sigma^2+2Dt}$. This illustrates the average effect created by the hemispherical distribution of the generated X-rays. The measured diffusion coefficient D^* is related to the true one D by [18]

$$D^* = D + \sigma^2/2t. \quad (8)$$

The same result was obtained by Ganguly *et al.* [17] under the same assumptions but with a more complicated derivation. It can be noted that Eq. (8) is an *exact* result with the assumptions of this section. The average effect is the most significant when the ratio $2Dt/\sigma^2 \ll 1$. Therefore, if σ is

identified by measurements across an ideal interface (or evaluated by considering the lateral spread of the electrons), a first order correction of the diffusion coefficient can be made by using Eq. (8). This correction may well predominate for low diffusion lengths. It can also be the first step of an iterative scheme that is based on a more complex model including absorption and fluorescence effects as presented in the following section. The case of a concentration-dependent diffusion coefficient can be treated in a similar way by considering it piecewise constant as would be assumed in any simple finite element discretisation.

Characteristic fluorescence across a concentration gradient

Theoretical developments

The effect due to the fluorescence in a homogeneous material is usually corrected by the formula derived by Reed [20, 21]. However, in the presence of a second phase in the area travelled by the X-rays emitted by the high atomic number material (B), fluorescence can occur in the other material (A). This leads to detecting X-rays of the element A where there should be only element B. Moreover, standard correction programs do not treat this problem. It is important to note that the same phenomenon occurs with the continuous background of the X-ray spectra and, contrary to characteristic X-rays, it concerns both materials. Earlier works have studied this problem [22, 23, 24] and Bastin *et al.* [25] have proposed a correction procedure in the case of two different alloys of A and B separated by an ideal interface. Yet, in all these studies, the results do not account for the effect of the primary emission volume crossing the interface between the two phases.

In this part, the average effect is directly included and the absorption effect is no longer neglected. However, the parameters of the 2D distribution function are not obtained by the required average but they are still assumed to be constant. This will not affect the final results since, for this case, the materials have very close depth and lateral distributions. The atom B stands for the element capable of producing K_β or K_α- radiations that can give rise to the K-shell ionisation of A. Let us consider an element $\mathrm{d}y\,\mathrm{d}z$ of the distribution function as a point source S emitting a part of the primary B-radiation, $\mathrm{dI}_\mathrm{B}^\mathrm{e}$, in the solid angle $\sin(\psi)\,\mathrm{d}\psi\,\mathrm{d}\varphi/4\pi$. Let M be the point of local spherical co-ordinates $(\mathrm{S}, r, \psi, \varphi)$. This point is located in the concentration profile by its co-ordinate $Y = \mathrm{d} + y + r\sin(\psi)\sin(\varphi)$. Along its way towards the point of interest, the primary elementary radiation is absorbed, according to Beer's

law, in a graded material. The intensity effectively seen at M is

$$\mathrm{dI_B(M)} = (\mathrm{p_{K_\beta}})\,\mathrm{dI^e_B(S)}\,\frac{\sin(\psi)\,\mathrm{d}\psi\,\mathrm{d}\varphi}{4\pi}\,\exp\left(-\int_{l=0}^{r}(\mu_{\mathrm{B}}^{\mathrm{AB}}\,\rho_{\mathrm{AB}})(\mathrm{d}+y+l\sin(\psi)\sin(\varphi))\,\mathrm{d}l\right), \quad (9)$$

where $\mathrm{p_{K_\beta}}$ stands for the relative transition probability of the $\mathrm{K_\beta}$ line [20, 26], when dealing with the $\mathrm{K_\beta}$ photons of B that are able to give rise to K-shell ionisation of A (*i.e.,* the only case for a Ni/Cu couple). Two computations have to be performed for two materials where the excitation of A by both $\mathrm{K_\alpha}$ and $\mathrm{K_\beta}$ lines of B occurs (*e.g.,* Zn/Ni couple). At M, both A and B-atoms absorb a radiation equal to $\mathrm{dI_B(M)}(\mu_{\mathrm{B}}^{\mathrm{AB}}\rho_{\mathrm{AB}})(Y)\mathrm{d}r$ and a fraction $\mathrm{C_A}(Y)\,\mu_{\mathrm{B}}^{\mathrm{A}}/\mu_{\mathrm{B}}^{\mathrm{AB}}(Y)$ is related to A-atoms. The latter is partly transformed into K-fluorescent radiation of A

$$\mathrm{dI^f_A(M)} = \omega_{\mathrm{A}}\left(\frac{r_{\mathrm{K}}-1}{r_{\mathrm{K}}}\right)_{\mathrm{A}}\mathrm{dI_B(M)}\,\mathrm{C_A}(Y)\,\frac{\mu_{\mathrm{B}}^{\mathrm{A}}}{\mu_{\mathrm{B}}^{\mathrm{AB}}(Y)}\,(\mu_{\mathrm{B}}^{\mathrm{AB}}\,\rho_{\mathrm{AB}})(Y)\,\mathrm{d}r, \quad (10)$$

where ω_{A} is the fluorescent yield and $((r_{\mathrm{K}}-1)/r_{\mathrm{K}})_{\mathrm{A}}$ the absorption edge jump ratio for the K-shell of element A [21]. Finally, this radiation emerges from the sample, at point N, to reach the spectrometer with a take-off angle θ and an angle δ wrt. the direction of the gradient (Fig. 1). Absorption occurs and the emerging intensity is

$$\mathrm{dI^f_A(N)} = \mathrm{dI^f_A(M)}\exp\left(-\int_{l=0}^{\frac{z+r\cos(\psi)}{\sin(\theta)}}(\mu_{\mathrm{A}}^{\mathrm{AB}}\,\rho_{\mathrm{AB}})(Y+l\cos(\theta)\cos(\delta))\,\mathrm{d}l\right). \quad (11)$$

Finally, the total emerging radiation for the point source S is obtained by integrating over r from 0 to ∞, ψ from 0 to $\cos^{-1}(-\min(1,z/r))$, since for a given radius $r > z$ this angle must be limited by the surface, and φ ranges from $-\pi$ to π. This last integration can be reduced by half thanks to the symmetry property of the problem. By dividing the intensity by the equivalent intensity obtained in a pure element A, $\mathrm{I_{(A)}}$, and integrating over the characteristic emission function leads to the k-ratio

$$\frac{\mathrm{I^f_A(d)}}{\mathrm{I_{(A)}}} = 2\int_{z=0}^{\infty}\int_{y=-\infty}^{\infty}\int_{r=0}^{\infty}\int_{\psi=0}^{\cos^{-1}(-\min(1,\frac{z}{r}))}\int_{\varphi=-\pi/2}^{\pi/2}\frac{\mathrm{dI^f_A(N)(d},y,z)}{\mathrm{I_{(A)}}}. \quad (12)$$

The dependence of the different absorption coefficients and density have to be expressed with the local mass fraction $\mathrm{C_A}(Y)$ by a simple rule of mixture [20] such as the elementary emission at S

$$\frac{\mathrm{dI^e_B(S)}}{\mathrm{I_{(A)}}} = \frac{\omega_{\mathrm{B}}}{\omega_{\mathrm{A}}}\,\frac{A_{\mathrm{A}}}{A_{\mathrm{B}}}\left(\frac{\mathrm{U_B}-1}{\mathrm{U_A}-1}\right)^{5/3}\frac{\Delta\,\phi(\rho z)\,g_\sigma(y)}{\mathrm{I_{(B)}}}\,(1-\mathrm{C_A}(y+\mathrm{d}))\,\mathrm{d}y\,\mathrm{d}\rho z, \quad (13)$$

where a simplified equation [22] is used to express the k-ratio, $\mathrm{I_{(B)}/I_{(A)}}$, of the primary intensities of the pure elements in the same analysis conditions, A_{X} and $\mathrm{U_X}$ stand respectively for the atomic weight and the overvoltage ratio of the element X. As mentioned in the previous part, the solution of

the equations that govern interdiffusion of two materials when the diffusion coefficient, D, is assumed to be constant leads to the following concentration profiles for a time t of diffusion

$$\mathrm{C_A}(Y) = \frac{1}{2}\left[1 + \mathrm{erf}\left(\frac{Y}{l_{\mathrm{diff}}}\right)\right], \tag{14}$$

where $l_{\mathrm{diff}} = 2\sqrt{Dt}$ corresponds to the diffusion length. The computation of the (characteristic) fluorescence for a Ni/Cu couple is shown in Fig. 3(b) for different diffusion lengths up to $l_{\mathrm{diff}} \to \infty$ corresponding to a homogeneous sample [21]. The maximum reached by the curve is due to a competition between the average effect that reduces the primary emission of B-atoms and the decrease in the absorption effect as the primary source becomes closer and closer to the A-rich phase. Moreover, this maximum shifts away from the interface when the diffusion length increases because the average effect on the primary B-radiations arises earlier (*i.e.*, for more important d values). Computations are performed with MATHEMATICA® on a PC. Computation times for twenty positions, d, vary from about half an hour for an ideal interface (see the following section) to less than ten minutes for a graded interphase region. The different integrations are estimated by a built-in algorithm that searches the best integration points for a required precision goal less than 1% of the value of the final integral.

Simplified concentration gradient and validations

For an ideal interface (*i.e.*, between two pure elements B and A), the mass fraction in A is described by a Heaviside step function located at $Y = 0$. By neglecting the part of the primary radiation which is directed towards the surface (*i.e.*, $\psi_{\max} = \pi/2$ instead of $\cos^{-1}(-\min(1, z/r))$ in Eq. (12)) yields the classical expression for fluorescence near an interface [22, 23, 24, 25] generalised to the case of a 2D characteristic emission function (instead of a point source) $\mathrm{I_A^{f\downarrow}(d)/I_{(A)}}$. It is worth remembering that $\mathrm{C_A} \neq 0$ only for $Y \geq 0$, *i.e.*, $r \geq -(\mathrm{d}+y)/\sin(\psi)\sin(\varphi)$. If the part of the primary radiation which is directed towards the surface, $\mathrm{I_A^{f\uparrow}(d)/I_{(A)}}$, has to be evaluated, Eq. (12) can be derived to obtain a similar expression as in Ref. [23]. The differences arise from the definition of the angle ψ (Fig. 1) and the 2D emission function. In the present development, it is important to note that there exists a relationship between r and ψ in Eq. (12) and it is easier, in this case, to replace the domain of integration by $-(\mathrm{d}+y)/\sin(\psi)\sin(\varphi) \leq r \leq z/\cos(\psi)$ and $\pi/2 \leq \psi \leq \pi/2 + \tan^{-1}(-z\sin(\varphi)/(\mathrm{d}+y))$.

These expressions allow for the comparison of the contribution of each radiation types (Fig. 3(b) for $l_{\mathrm{diff}} = 0\mu\mathrm{m}$). If the upper radiation is negligible [23] when the beam is not too close to the interface (such as in a homogeneous sample), then it becomes important near the maximum of the secondary

emission. It can reach up to 20% of the total secondary emission for Ni/Cu couple. Moreover, the previous equation includes the average effect on the primary emission of B. This leads to significant differences between the results derived herein and those obtained with a point source [22, 23, 24, 25] when d is close to 0. To compare the derived equations with actual measurements, the average effect on the global scale (as discussed in the first section) must be added. The assumption on the absorption effect made in the first section is no longer made and Eq. (3) is computed to simulate the average effect. Yet, the quantity σ is identified with the B-intensity by using Eq. (4). WDS measurements ($\mathrm{K}_{\alpha 1}$ on CAMECA SX50) have been carried out on a Ni/Zn couple (with significant characteristic fluorescence, since $\mathrm{Z}_{\mathrm{Zn}} - \mathrm{Z}_{\mathrm{Ni}} = 2$, with K_{α} and K_{β} lines [20]) obtained by carefully clamping together with a simple screw the polished surfaces of each material, followed by cutting the sample perpendicular to the interface and polishing the complete assembly parallel to the interface. Note that an inclined spectrometer was used to reduce any crystal defocusing due to the secondary X-rays generated at a significant distance from the electron beam as well as the one arising from the possible (but weak) long range undulations and imperfections of the surface. Comparisons between measured and predicted profiles given in Fig. 4 show a good agreement for a Ni/Zn couple.

Because the specimen stage minimum displacement of the microprobe used is equal to one micrometer (*i.e.*, the beam step mode was not used), the average effect is not well identified. Other measurements (PGT EDS on HITACHI S510 SEM) have been performed on the same sample. These two techniques are complementary since the first one gives the best intensity measurements and the second a lower displacement step. Note that the average effect is more important, as mentioned earlier, in WDS measurements since the probe current is much higher than in the SEM (more than fifty times higher in our case). Therefore σ for the WDS technique is twice larger than for the SEM/EDS with the same acceleration voltage. This result shows the importance of the beam diameter in the lateral spread of the electrons. Other validations have been performed on Ni/Cu couple (characteristic fluorescence only involving the K_{β} line of copper, since $\mathrm{Z}_{\mathrm{Cu}} - \mathrm{Z}_{\mathrm{Ni}} = 1$ [20]), and these computations have been compared to measurements. Moreover, simulations for a Co/Cu couple have been performed to check the fluorescence computation for high values of d by comparing them with other results [25]. It should be remembered that none of these computations consider the continuum fluorescence. It can explain the (weak) difference between simulations and measurements in Fig. 4 since the simulations underestimate the real k-ratio. The continuum excited fluorescence appears for both A and B (and it can be

clearly observed with a logarithmic scale on WDS measurements) and can be reasonably simulated by a point source approximation [20, 22, 24, 27] or with a 2D distribution function based on the use of the depth distribution function for the continuous radiation [28, 29]. Lastly, the continuum fluorescence is of the same order as the K_β characteristic fluorescence for diffusion couples such as Ni/Cu or Ni/Zn with $\mathrm{E}_0 \sim 25\mathrm{keV}$ [24].

Conclusion

All the effects described herein have a non negligible influence on the evaluation of diffusion coefficients when the diffusion length is of the same order of magnitude as the lateral spread of the electrons and the X-rays. For example, the average effect amplifies the diffusion coefficient or can lead one to conclude that some diffusion has occurred when it has not (therefore, one may call them measurement 'artefacts'). Diffusion coefficients are, in most cases, dependent on the local concentration and fluorescence adds a strong dependence of the diffusion coefficient with low concentrations in an A-element that can yield false conclusions regarding the diffusion dependence on other parameters (such as stresses). The equations proposed herein allow for the deconvolution of the real concentration profile from the raw measurements by an iterative scheme. This is possible because computation times are negligible compared to Monte Carlo methods proposed to solve this kind of problem [30, 31]. However, these approaches, in particular those in which the electrons as well as the radiation paths are simulated [31], are more realistic and accurate (if numerous electrons are simulated) and include all the effects encountered during a concentration profile measurement. However, they need high computation capacity and are still long and difficult to integrate in a correction procedure.

Acknowledgements. The authors wish to thank Mr M. Spirckel for the WDS measurements made possible on a CAMECA SX50 at the Centre Technique d'Arcueil (France).

References.

[1] D.B. Wittry, J. Appl. Phys., 1958, 29(11), 1543.

[2] P. Duncumb, in: 2^{nd} International Symposium on X-ray Microscopy and X-ray Microanalysis (A. Engström, V.E. Cosslett, H.H. Pattee, Eds.), Elsevier, Amsterdam, 1960, 365.

[3] S.J.B. Reed, in: 4^{th} International Conference on X-ray Optics and Microanalysis (R. Castaing, P. Deschamps, J. Philibert, Eds.), Hermann, Paris, 1966, 339.

[4] D.C. Joy, Monte Carlo Modelling for Electron Microscopy and Microanalysis, Oxford University

Press, Oxford, 1995.

[5] K.F.J. Heinrich, Electron Beam X-ray Microanalysis, Van Nostrand Reinhold Company, New York, 1981.

[6] R.H. Packwood, D.J. Brown, X-Ray Spectrom., 1981, 10(3), 138.

[7] D.J. Brown, R.H. Packwood, X-Ray Spectrom., 1982, 11(4), 187.

[8] G.F. Bastin, H.J.M. Heijligers, F.J.J. van Loo, Scanning, 1986, 8(2), 45.

[9] J. Riveros, G. Castellano, X-ray Spectrom., 1993, 22, 3.

[10] P. Hovington, D. Drouin, R. Gauvin, Scanning, 1997, 19, 1.

[11] D. Drouin, P. Hovington, R. Gauvin, Scanning, 1997, 19, 20.

[12] P. Hovington, D. Drouin, R. Gauvin, D.C. Joy, N. Evans, Scanning, 1997, 19, 29.

[13] I. Barkshire, P. Karduck, W.P. Rehbach, S. Richter, Mikrochim. Acta, 2000, 132(2-4), 113.

[14] J.C. Russ, in: A.S.T.M. S.T.P. 485, A.S.T.M., Philadelphia, 1971, 154.

[15] R. Castaing, Ph.D. Thesis, University of Paris, 1951. O.N.E.R.A. Publication 55, 1952.

[16] C.C. Lo, D.E. Schuele, J. Appl. Phys., 1975, 46(11), 5004.

[17] J. Ganguly, R.B. Bhattacharya, S. Chakraborty, Am. Mineral., 1988, 73, 901.

[18] O. Arnould, F. Hild, Microscopy and Analysis, 2000, 66, 13 (European Edition), 25 (Americas Edition).

[19] G.F. Bastin, F.J.J. van Loo, H.J.M. Heijligers, X-Ray Spectrom., 1984, 13(2), 91.

[20] S.J.B. Reed, Electron Microprobe Analysis, Cambridge University Press, Cambridge, 1975.

[21] S.J.B. Reed, Brit. J. Appl. Phys., 1965, 16, 913.

[22] S.J.B. Reed, J.V.P. Long, in: 3^{rd} International Conference on X-ray Optics and Microanalysis (H.H. Pattee, V.E. Cosslett, A. Engström, Eds.), Academic Press, New York, 1963, 317.

[23] F. Maurice, R. Seguin, J. Henoc, in: 4^{th} International Conference on X-ray Optics and Microanalysis (R. Castaing, P. Deschamps, J. Philibert, Eds.), Hermann, Paris, 1966, 357.

[24] J. Henoc, F. Maurice, A. Zemskoff, in: 5^{th} International Conference on X-ray Optics and Microanalysis (G. Möllenstedt, K.H. Gaukler, Eds.), Springer, Berlin, 1969, 187.

[25] G.F. Bastin, F.J.J. van Loo, P.J.C. Vosters, J.W.G.A. Vrolijk, Scanning, 1983, 5, 172.

[26] K.F.J. Heinrich, C.E. Fiori, R.L. Myklebust, J. Appl. Phys., 1979, 50(9), 5589.

[27] J. Trincavelli, G. Castellano, J.A. Riveros, X-Ray Spectrom., 1998, 27, 81.

[28] H.J. August, J. Wernisch, Scanning, 1991, 13, 207.

[29] A. Pfeiffer, C. Schiebl, J. Wernisch, X-Ray Spectrom., 1996, 25, 131.

[30] R.L. Myklebust, D.E. Newbury, Scanning, 1995, 17, 235.

[31] X. Llovet, E. Valovirta, E. Heikinheimo, Mikrochim. Acta, 2000, 132, 205.

Footnotes.

* To whom correspondence should be addressed - Email: Olivier.Arnould@lmt.ens-cachan.fr.

[1] Download site: ftp://freebie.engin.umich.edu/pub/MSA+MAS/MMSLib/Monte/Joy/

[2] Download site: http://vulcain.gme.usherb.ca/casino/

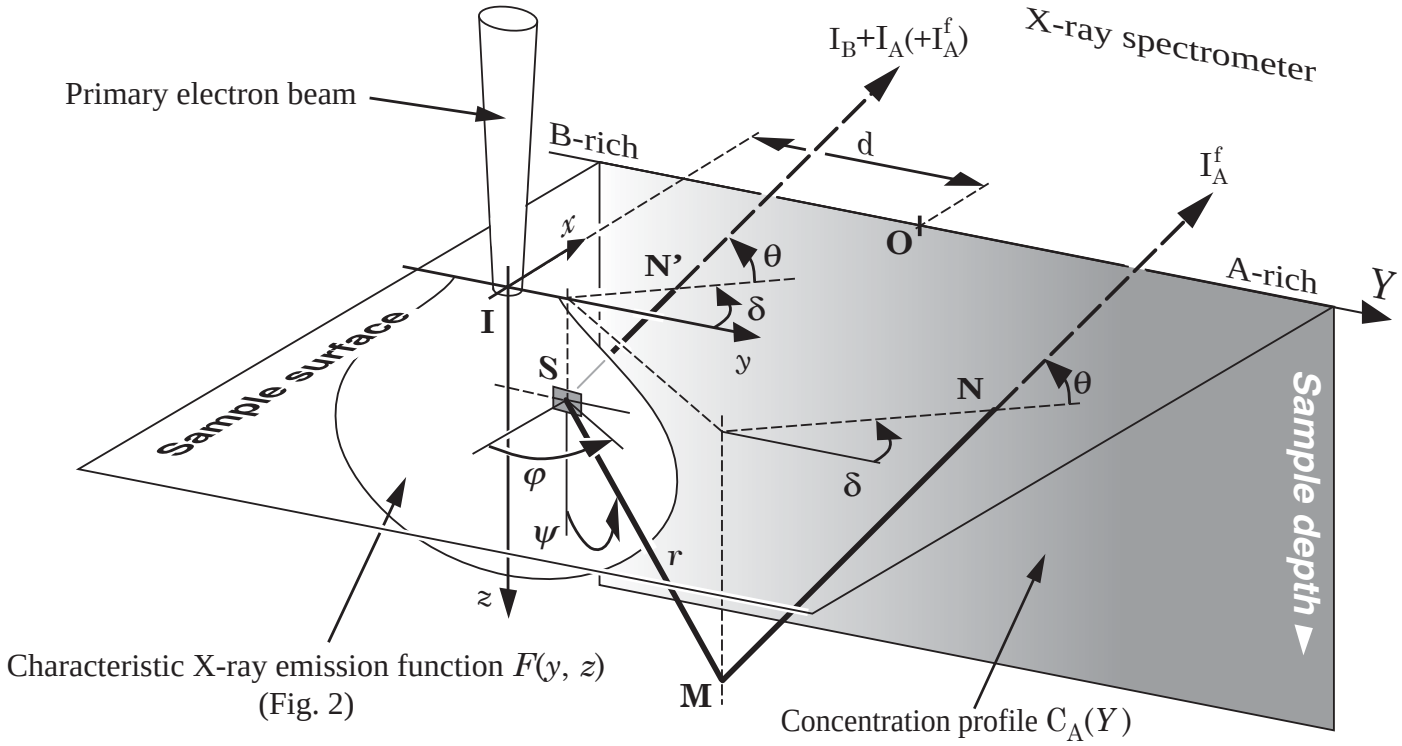

Figure 1: Schematic of the entire process of characteristic fluorescence and average effect in a concentration profile $\mathrm{C_A}(Y)$ of mixed A and B elements. The change in concentration is depicted by the grey level (the darker, the richer in A-atoms). An electron beam is focused at a point I on the sample surface at a distance d from the origin, $Y = 0$, of the concentration curves O. The spread of the electrons in the sample produces a 3D characteristic emission of X-rays that reduces to a 2D function in the present case $F(y, z)$. Each point, S of this distribution generates A and B primary X-rays that emerge from the sample surface at N' to reach the spectrometer that detects their intensity, $\mathrm{I_A}$ and $\mathrm{I_B}$. B-radiations are absorbed in the material and can produce secondary excitation of A-atoms (since $\mathrm{Z_B} > \mathrm{Z_A}$) at M. The generated fluorescent radiations emerge from the sample surface at N to reach the spectrometer that detects their intensity $\mathrm{I_A^f}$.

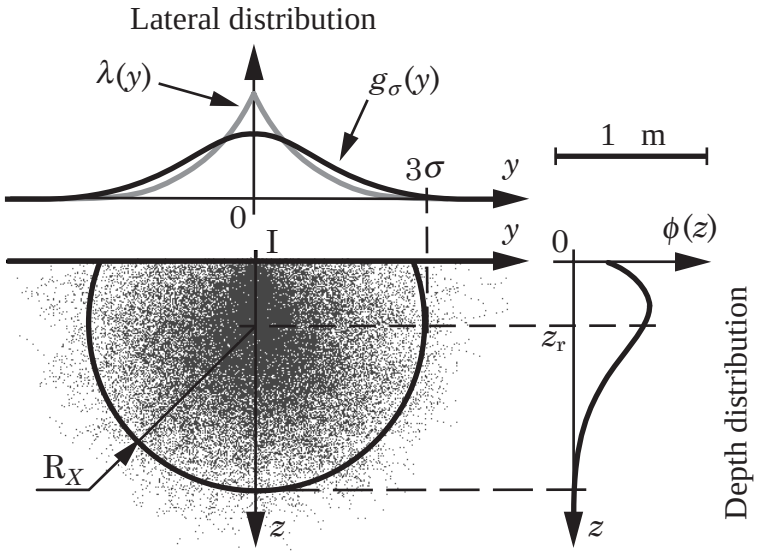

Figure 2: X-ray emission volume in copper obtained by Monte Carlo simulations [4][1] when $\mathrm{E}_0 = 25\mathrm{keV}$ with an electron probe diameter of $10\mathrm{nm}$. Definition of the lateral, with the real distribution $\lambda(y)$ and its Gaussian approximation $g_\sigma(y)$, and depth, $\phi(z)$, X-ray distributions.

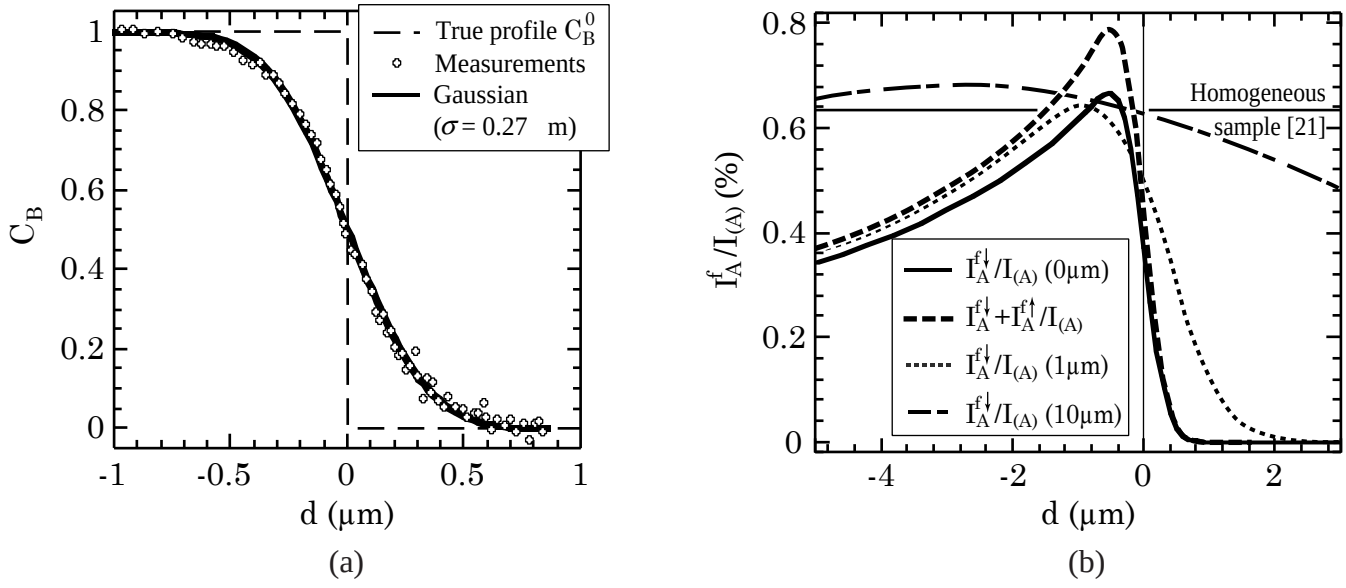

Figure 3: (a) Average effect for an ideal interface Ni(A)/Cu(B). Measurements obtained by EDS with $\mathrm{E}_0 = 25\mathrm{keV}$, $\theta = 27°$, $\delta = \pi/2$. (b) Simulation of fluorescence vs. beam position d for different diffusion lengths l_{diff} for a Ni(A)/Cu(B) couple with $\sigma = 0.27\mu\mathrm{m}$, $\mathrm{E}_0 = 25\mathrm{keV}$, $\theta = 40°$ and $\delta = \pi/2$.

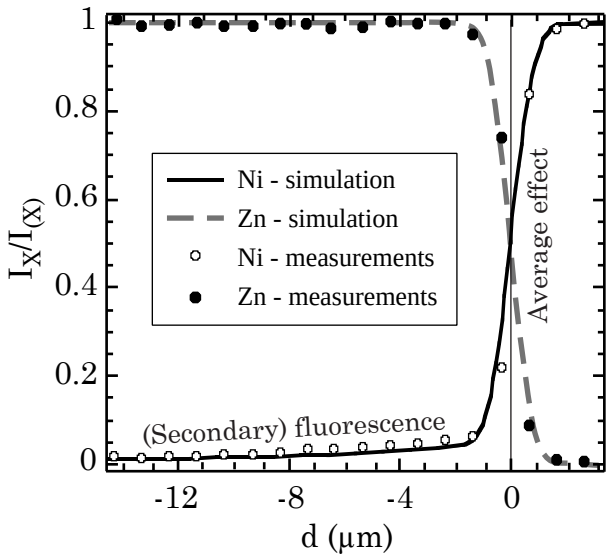

Figure 4: Apparent experimental (WDS) and predicted concentration $(\mathrm{I_X} + \mathrm{I_X^f})/\mathrm{I_{(X)}}$ vs. beam position d from the interface of a Ni(A)/Zn(B) couple with $\sigma = 0.6\mu\mathrm{m}$, $\mathrm{E_0} = 19.7\mathrm{keV}$, $\theta = 40^\circ$ and $\delta = 7\pi/12$.